RESEARCH ARTICLE | JULY 23 2021

Experimental observation of the geodesic acoustic frequency limit for the NBI-driven Alfvén eigenmodes in TJ-II

L. G. Eliseev ; A. V. Melnikov ; E. Ascasibar ; A. Cappa ; M. Drabinskiy; C. Hidalgo ; P. O. Khabanov ; N. K. Kharchev ; A. S. Kozachek; M. Liniers ; S. E. Lysenko ; M. Ochando ; J. L. de Pablos ; I. Pastor ; S. E. Sharapov ; D. A. Spong ; B. N. Breizman ; J. Varela

Phys. Plasmas 28, 072510 (2021)
https://doi.org/10.1063/5.0049225
CHORUS

Physics of Plasmas ARTICLE scitation.org/journal/php

Experimental observation of the geodesic acoustic frequency limit for the NBI-driven Alfvén eigenmodes in TJ-II

Cite as: Phys. Plasmas **28**, 072510 (2021); doi: 10.1063/5.0049225
Submitted: 3 March 2021 · Accepted: 3 July 2021 ·
Published Online: 23 July 2021

L. G. Eliseev,[1] A. V. Melnikov,[1,2] E. Ascasibar,[3] A. Cappa,[3] M. Drabinskiy,[1] C. Hidalgo,[3] P. O. Khabanov,[1] N. K. Kharchev,[1,4] A. S. Kozachek,[5] M. Liniers,[3] S. E. Lysenko,[1,a)] M. Ochando,[3] J. L. de Pablos,[3] I. Pastor,[3] S. E. Sharapov,[6] D. A. Spong,[7] B. N. Breizman,[8] and J. Varela[9]

AFFILIATIONS

[1]Tokamak Division, National Research Centre "Kurchatov Institute," 123182 Moscow, Russia
[2]Institute for Laser and Plasma Technologies, National Research Nuclear University "MEPhI," 115409 Moscow, Russia
[3]Fusion National Laboratory, CIEMAT, 28040 Madrid, Spain
[4]Prokhorov General Physics Institute, Russian Academy of Science, 119991 Moscow, Russia
[5]Institute of Plasma Physics, NSC KIPT, 310108 Kharkov, Ukraine
[6]CCFE, Culham Science Centre, Oxfordshire OX14 3DB, United Kingdom
[7]Oak Ridge National Laboratory, Oak Ridge, Tennessee 37831-6169, USA
[8]Institute for Fusion Studies, University of Texas at Austin, Austin, Texas 78712-1203, USA
[9]Universidad Carlos III de Madrid, 28911 Leganés, Madrid, Spain

[a)]**Author to whom correspondence should be addressed:** lysenksergej@yandex.ru

ABSTRACT

We study Alfvén eigenmodes (AEs) in the TJ-II heliac in hydrogen plasmas heated by hydrogen co-field neutral beam injector. Taking advantage of the unique TJ-II flexibility in a varying plasma current, we have observed strong variation of the AE frequency from $f_{AE} \sim 30$ to ~220 kHz for selected modes. An advanced heavy-ion beam probe diagnostic determines the spatial location and internal amplitudes of the modes. The modes satisfy a local AE dispersion relation including the geodesic acoustic frequency that represents the lowest frequency of the mode. Linear MHD modeling with STELLGAP and FAR3D codes shows that the calculated temporal evolution of the mode frequency reproduces the observed maxima and minima at the same time intervals with a similar frequency range, and the radial profile peaks near the outer edge of the observed one.

I. INTRODUCTION

Alfvén eigenmodes (AEs) are extensively studied in both tokamaks and stellarators, and overviews of recent results are presented in Refs. 1–3. Low magnetic shear TJ-II stellarator plasmas are especially relevant for the advanced tokamak scenario, requiring off-axis non-inductive current drive and leading to a broad region of low magnetic shear. Fast ion-driven Alfvén instabilities in low-density plasmas of TJ-II are frequently observed in the form of chirping modes with bursting amplitudes and sweeping frequencies in the range 100–350 kHz.[4–7] In the neutral beam injector (NBI)-only heated plasmas at higher densities in TJ-II, both chirping and continuous modes[8] were observed with frequencies in the range 50–300 kHz interpreted as helicity-induced Alfvén eigenmodes (HAEs) and global Alfvén eigenmodes (GAEs). Recent experiments in TJ-II have revealed that the frequency of AEs, f_{AE}, is linked to the plasma current I_{pl} in a shot-to-shot configuration scan.[9]

The HAE's frequencies are known to be associated with gaps in the Alfvén continuum in the presence of couplings between various toroidal and poloidal harmonics. Unlike HAEs, the GAEs do not necessarily require harmonic coupling for their existence. The underlying reason for them is a nearly flat radial dependence of the local Alfvén frequency for an individual harmonic. In the GAE case, this feature is due to the plasma density profile. Similarly, the local Alfvén frequency is a weak function of the radius near shear reversal points, which is the

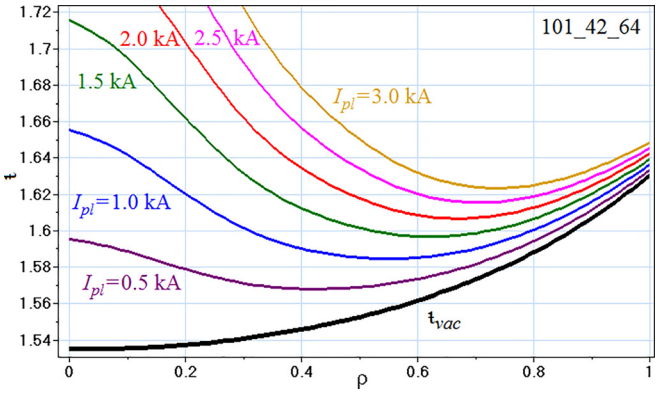

FIG. 1. Rotational transform profiles with the presence of plasma current I_{pl} in TJ-II. Fat black line denotes the initial profile of ι_{vac} with $I_{pl} = 0$.

physics reason behind the so-called Alfvén Cascades[10] aka RSAEs (reversed shear Alfvén modes).[11] This is the case for the mode of interest in our paper.

It was predicted theoretically,[10] calculated by gyrokinetic code for the DIII-D tokamak,[12] and observed experimentally in LHD[13] and in DIII-D[11] that in low-beta plasmas the lower limit of f_{AE} is the geodesic acoustic mode (GAM) frequency f_{GAM}.

The present paper complements the LHD results by independent measurements on TJ-II. The TJ-II has an almost flat vacuum iota profile. In this study, we also make use of the unique capability of the heavy-ion beam probe (HIBP) to measure local electrostatic and magnetic perturbations associated with Alfvén eigenmodes.[14] Experimental results are analyzed with MHD codes STELLGAP,[15] which calculates the structure of the Alfvén continuum and gaps, and FAR3D,[16,17] which gives the AE radial location and frequency time evolution. Equilibrium for both codes is reconstructed with VMEC code.[18]

II. EXPERIMENTAL SETUP

The experiments described in this paper have been performed on the four-period TJ-II heliac with volume averaged major and minor radii $\langle R \rangle = 1.5$ m and $\langle a \rangle = 0.22$ m correspondingly. The on-axis magnetic field was $B_0 = 0.95$ T, the vacuum magnetic configuration has rather flat iota profiles.[19] The details of the experimental setup were presented in the paper,[20] but for clarity, we briefly repeat the main points. Due to the unique capability to change independently the currents in the magnetic field coils, TJ-II is able to vary the vacuum rotational transform ι_{vac} from shot to shot in an extended range: $0.9 < \iota_{vac}(0) < 2.5$ ($\iota = 1/q$). Figure 1 shows with a thick black line of the flat profile of the vacuum rotational transform ι_{vac} for the configuration under study 101_42_64 [configuration label means the currents in the circular coil (CC), helical coil (HX), and vertical field coils (VF), I_{CC}_I_{HX}_ I_{VF} shown in kA/10]. The iota profiles were calculated with the approximate formula based on the MHD equilibrium modeling, which assumes Spitzer resistivity and radially constant loop voltage for the plasma current density, and works well for a wide range of plasma currents $|I_{pl}| < 8.5$ kA.[21] Numerous studies of AEs in TJ-II with this model, showing the good agreement between modeling results and

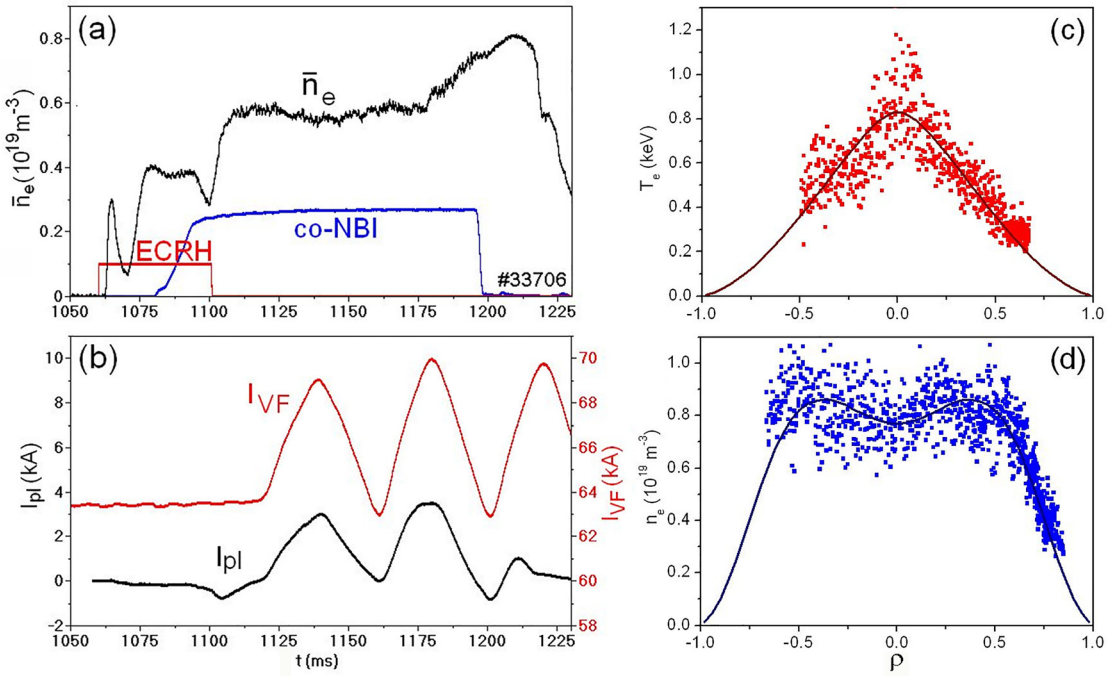

FIG. 2. Discharge scenario and electron density and temperature profiles. Magnetic configuration 101_42_64, $P_{ECRH} = 0.5$ MW, $P_{NBI} = 0.5$ MW, co-injection. (a) Discharge scenario; (b) the waveform of the current in the vertical field coils I_{VF} and induced plasma current I_{pl}; radial profiles for electron temperature (c) and density (d) for NBI phase of the discharges measured in the series of the similar shots by Thomson scattering, $\bar{n}_e = 0.57 \times 10^{19}$ m^{-3}.

observations,[20,22–24] allow us to estimate the accuracy of the reconstructed iota profiles as low as a few percent.

The hydrogen plasmas were heated with up to 0.3 MW on- and off-axis electron cyclotron resonance heating (ECRH) at the second harmonic X-mode at 53.2 GHz. One or two neutral beam injectors (NBI) injected hydrogen particles at 32 keV (Ref. 25) with H ion velocities $V_{NBI} \sim 2.5 \times 10^6$ m/s, which is about one third of the Alfvén velocity for the experiments discussed in this paper. Most of the presented experiments were performed with these plasmas, in which we dynamically varied the current I_{VF} to vary the rotational transform, as shown in Fig. 1.

Figure 2 shows a time evolution of the plasma parameters with a periodic variation in the plasma current, discussed in this paper. There are three heating phases in the discharge: ECRH only, ECRH + NBI, and NBI-only. NBI is co-directed relative to the equilibrium magnetic field.[26] During the ECRH + NBI and NBI-only phases, the plasma density could be kept more or less constant, as the Li coating of the first wall balances the NBI fueling, chamber wall outgassing, and ECRH-induced density pump-out.[27] However, in the NBI-only phase, the plasma density increases somewhat as a result of fueling by the beams. The initially hollow electron density profile becomes flat and then evolves into a parabolic shape.

The diagnostics consisted of a poloidal array of 24 magnetic Mirnov probes (MP) inside the vacuum vessel for the measurement of magnetic flux oscillation just outside the plasma.[28] The plasma current $I_{pl}(t)$ was measured by Rogowski coil, and line-averaged density $\bar{n}_e(t)$ was measured by interferometry. We also used a multi-chord bolometer array[29] and a heavy-ion beam probe (HIBP).[30–32] Bolometers measure the plasma emission in a 2 eV to 4 keV energy range along 16 chords covering the whole plasma column, $-1 < \rho < 1$, where ρ is a normalized minor radius.

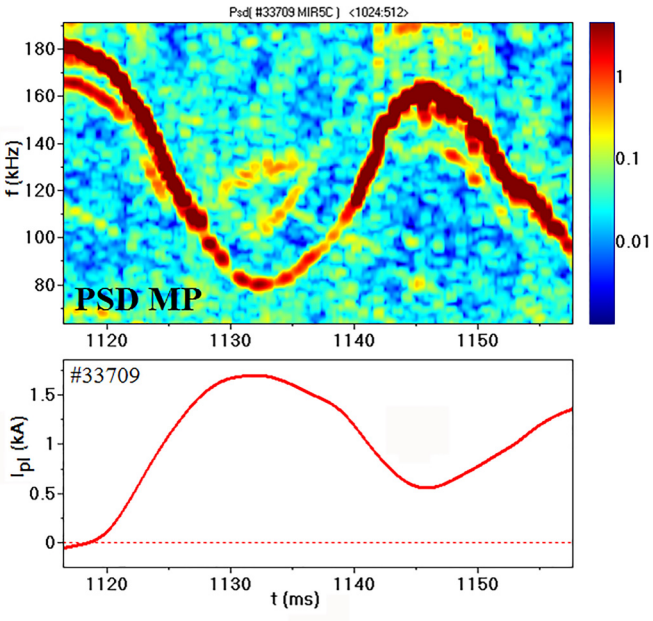

FIG. 3. Monotonic dependence of the mode frequency f_{AE} on plasma current I_{pl}. Local extrema of f_{AE} correspond to local extrema of I_{pl}. Top: power spectral density of magnetic perturbation by Mirnov probe (MP); bottom: time trace of I_{pl}.

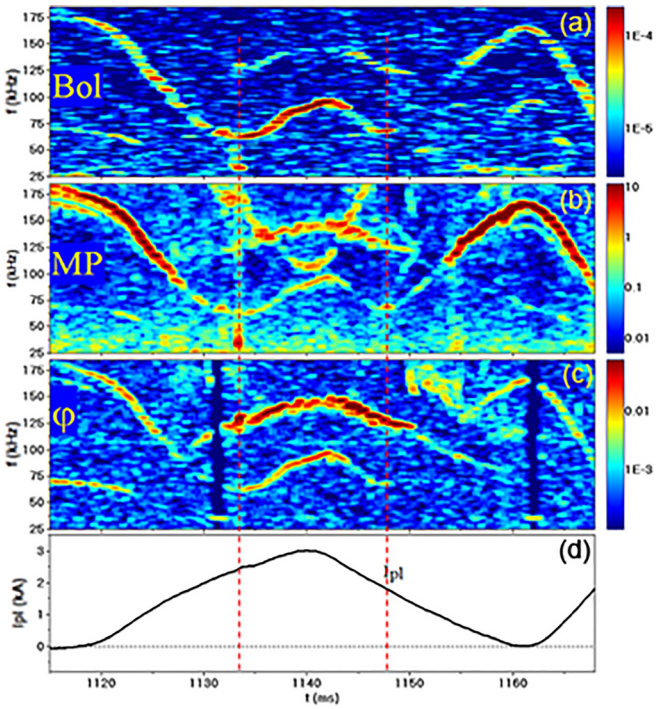

FIG. 4. Mode frequency evolution, showing the occurrence of local minima during the linear evolution of I_{pl} for the selected Alfvén eigenmode with local minima (AELM). Power spectral densities of the plasma emission by the central chord of bolometer $\rho_{Bol} = 0.1$ (a); magnetic perturbation by Mirnov probe (MP) (b); and plasma potential by HIBP, $\rho_{HIBP} = 0.35$ (c); time trace of I_{pl} (d). Time instants of the local minima for AELM are marked by vertical dashed lines.

HIBP measures simultaneously the local mean and oscillatory plasma electric potential and density, as well as magnetic potential oscillations.[33] We used the HIBP to measure the internal amplitudes of the energetic particle (EP)-driven modes and determine whether the oscillations are predominantly electrostatic or electromagnetic.[34] Cs^+ primary ions were injected with initial energy $E_b \leq 127$ keV. The local plasma potential φ_{pl}^{SV} was measured in a sample volume (SV) with a radial length of about 1 cm.[35]

At the density range under study, $\bar{n}_e < 1 \times 10^{19}$ m^{-3}, the probing beam attenuation is low and the secondary beam current I_t describes the plasma density in the sample volume n_e^{SV}. For higher densities,

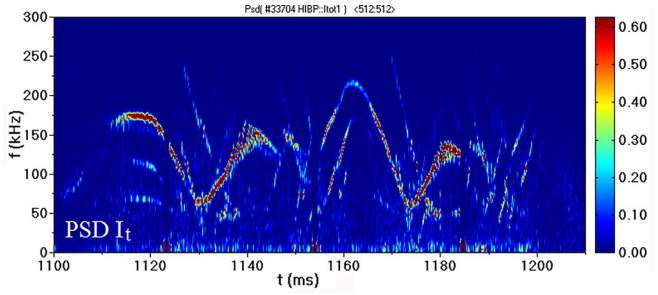

FIG. 5. An example of the lower frequency limit for multiple AEs. HIBP density spectrogram, #33704.

the attenuation factors along the beam trajectories need to be taken into account and a profile reconstruction becomes necessary.[36]

The oscillations of beam toroidal position in the detector ζ_d represent the oscillatory component of magnetic potential.[37] The AEs were evident in all three parameters measured by HIBP,[14] and we use all of them in the present analysis with an emphasis on the plasma potential and density oscillations. HIBP measures AEs in TJ-II with a radial resolution of ~1 cm over the whole plasma cross section $-1 < \rho < 1$, with the convention that $\rho < 0$ for the high field side (HFS) and $\rho > 0$ for the low field side (LFS) of the plasma. We used the HIBP to measure the time-dependent signals at a fixed radial position for the *SV* at a sampling rate of 1 MHz and bandwidth of 300 kHz. A radial profile is obtained in equivalent shots by changing the SV position ρ_{HIBP}.

III. MODE BEHAVIOR IN DISCHARGES WITH VARIABLE PLASMA CURRENT

In TJ-II, there is an effective way to vary the AE frequency by changing B_{VF} (I_{VF}).[20] The following scenario was explored: Co-NBI + sawtooth I_{VF} variations during one shot with initial configuration labeled as 101_42_64 with $\iota_{\mathrm{vac}}(0) = 1.53$ and shown by the black fat line in Fig. 1.

An example of the AE frequency evolution with I_{VF} is presented in Fig. 3. I_{VF} variation does not change vacuum iota ι_{vac}, but induces I_{pl} changes, therefore the changes in magnetic configuration. Decreasing I_{VF} by 10% induces about a 1.5 kA increase in I_{pl}, which in turn leads to a mode frequency decrease by a factor of 2. In Fig. 3, the AE frequency mirrors the evolution of I_{pl}: an increase/decrease in I_{pl} results in a decrease/increase in f_{AE}. However, the mode frequencies do not always depend on the current monotonically. An example of that is shown in Fig. 4. In this figure, there is a time interval in which I_{pl} changes linearly, but the mode frequency still has a local minimum. To separate such modes from others, we call them the Alfvén eigenmode with local minima (AELM). The experiment shows that f_{AE} never reaches zero. There are only two possibilities for the AEs with decreasing frequency: the mode frequency either increases after the local minimum or the mode disappears altogether. The experimental range of the minimum frequencies is from 30 to 60 kHz, depending on the plasma scenario (see Figs. 4 and 5). We note that during the evolution of the I_{pl}, the mode may change the character from the steady-frequency form to the chirping form and back.[22]

To interpret the observed correlation between the mode frequency and the plasma current, we use a local dispersion relation from Ref. 10, which involves the geodesic acoustic mode frequency

$$f_{AE}^2(\rho, t) = \left(\frac{1}{2\pi R}\left|m\iota(\rho, t) - n\right| V_A\right)^2 + f_{GAM}^2, \tag{1}$$

where ι is taken as[20]

$$\iota(\rho, t) = \iota_{vac}(\rho) + C(\rho) I_{pl}(t) + \delta\iota, \tag{2}$$

where m, n, and $\delta\iota$ are fitting parameters; values of m, n are typically limited to be ≤ 17; $C(\rho)$ is a fixed function, determined as a result of MHD modeling;[21] and f_{GAM} was defined in accordance with Ref. 13, where the factor $7/4 \cdot T_i$ was at first introduced in Ref. 38

$$f_{GAM}(\rho) = \frac{1}{2\pi R}\sqrt{\frac{\left(T_e + \frac{7}{4}T_i\right)}{m_i}\left(2 + \frac{1}{q^2}\right)} = \frac{1}{2\pi R}\sqrt{\frac{\left(T_e(\rho) + \frac{7}{4}T_i(\rho)\right)}{m_i}\left(2 + \iota^2(\rho)\right)}. \tag{3}$$

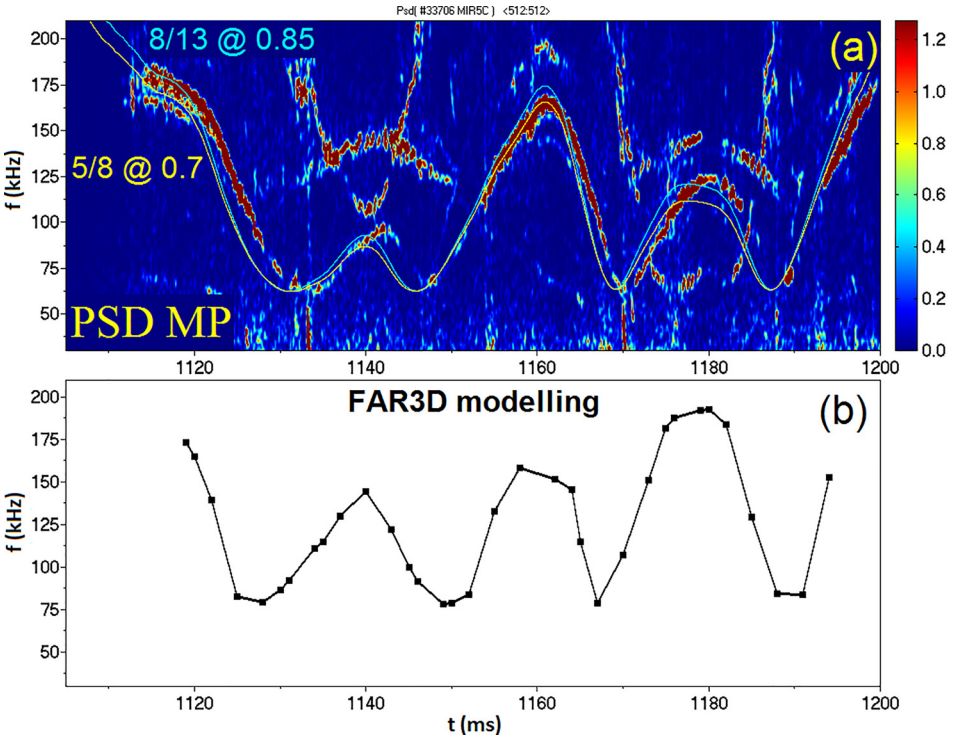

FIG. 6. (a) Power spectrogram of magnetic fluctuations measured by Mirnov probe in comparison with the analytical prediction by Eqs. (1)–(3) for $f_{min} = f_{GAM} = 62$ kHz: 8/13@$\rho_{AELM} = 0.85$ in blue and 5/8@$\rho_{AELM} = 0.7$ in yellow. Both curves reproduce the observed time evolution of f_{AELM}; local minima at $t = 1130$, 1145, 1170, and 1185 ms correspond to $(m\iota - n) = 0$ in Eq. (1); (b) modeling of the AELM frequency by the FAR3D code results in 5/8 mode, which reproduces the mode frequency sweeping.

We herein use an approximate expression for f_{GAM} as an estimate that is applicable to non-axisymmetric systems as long as toroidicity rather than helical harmonics determines the geodesic magnetic curvature. However, calculations for a similar unperturbed magnetic configuration (100_44_64) show that the helical components are not negligibly small and should generally be taken into account.[39] A more general calculation of the GAM frequency can be found in Refs. 40 and 41.

It was shown in Ref. 11 that the local EC heating can affect RSAE frequency due to the pressure gradient effect. Estimations show that this effect in TJ-II is small [contribution to Eq. (1) <1%] because the thermal plasma beta is quite low.

Figure 6(a) compares the magnetic spectrogram and the result of the modeling (1–3) for the frequency pattern in the experiments with I_{pl} variation. In this shot #33706, a single mode lasts about 90 ms, which is a lifetime record for AE's in TJ-II. The mode frequency varies from 62 to 175 kHz due to I_{pl} variation from −0.5 to 2.5 kA at the constant density. Figure shows that there are two modeled modes, $m/n = 5/8$ at $\rho_{AELM} = 0.7$ (yellow line) and $m/n = 8/13$ at $\rho_{AELM} = 0.85$ (blue line) shown by thin curves on top of the magnetic spectrogram, that reproduce observed frequency evolution.

Figure 6(b) presents the FAR3D modeling of AELM frequency, reproducing the frequency sweeping during the AELM lifetime for the mode $m/n = 5/8$. The numerical model itself will be discussed in Sec. IV. The mode $m/n = 5/8$ obtained with model (1–3), presented in yellow in Fig. 6(a), coincides with the FAR3D outcome.

Figures 7(a)–7(f) shows the spatial distribution of the plasma potential (φ) and density (I_t) perturbations, caused by AELM, observed during HIBP spatial scans. We chose the scans, in which AELM lasts during the whole scanning period, as proven by Mirnov data. Figures 7(a)–7(c) shows that the mode is radially extended, and density is perturbed from nearly plasma center to $\rho = 0.85$. Plasma potential is also perturbed almost from $\rho = 0$ up to the outer limit of the measurements, determined by the signal-to-noise ratio, which is about 0.75–0.8, as shown in Figs. 7(d)–7(f). Figure 7 also shows that the density and potential perturbations have some deviation between each other and LFS–HFS. By average, we may estimate the area of most pronounced density perturbation as $\rho_{AELM} = 0.4 \pm 0.25$, while for plasma potential it is located more outer at 0.6 ± 0.25 for LFS, and for HFS, it is the same, but less pronounced (20 V in HFS against 60 V in LFS). Figure 7(g) shows the eigenfunction of the perturbed

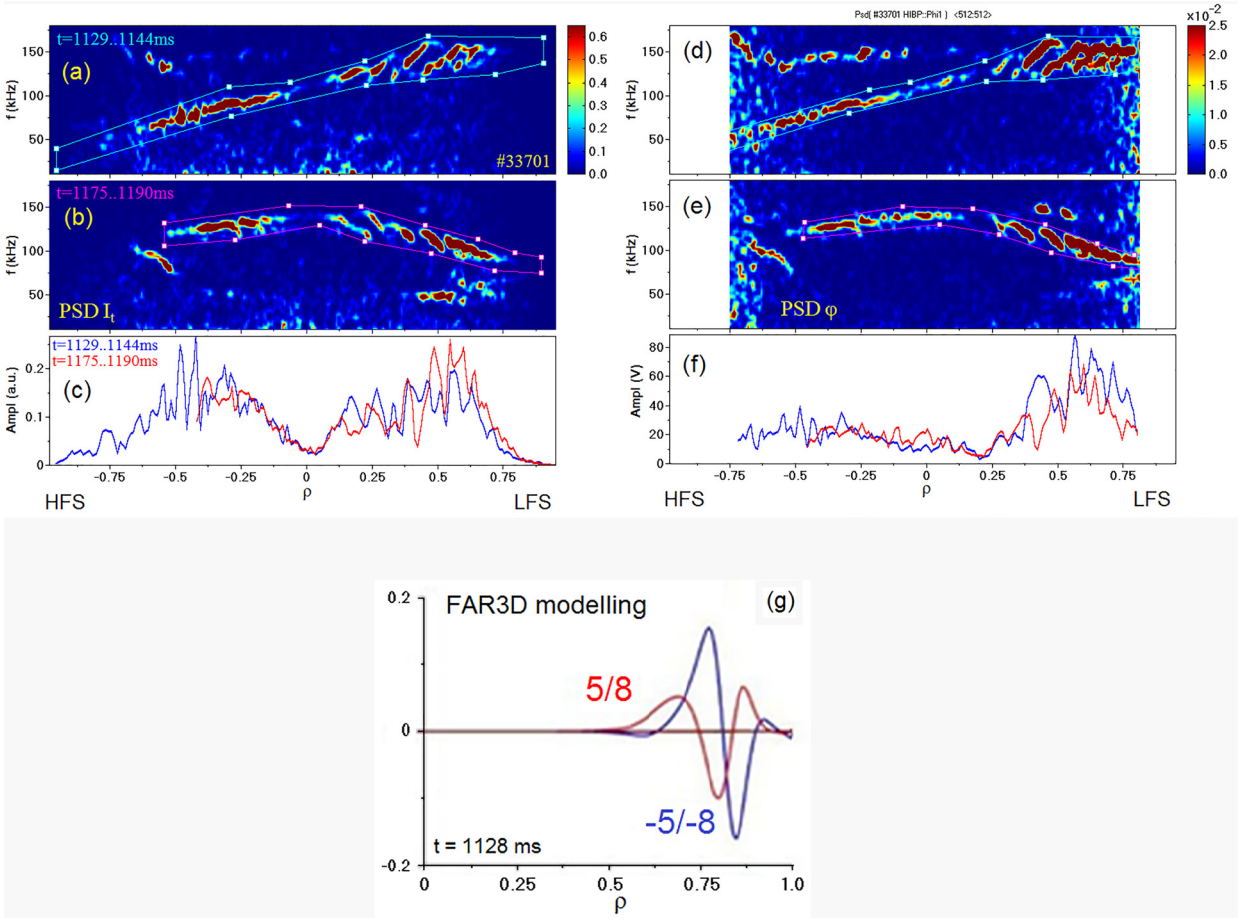

FIG. 7. Radial profile of the AELM obtained with the HIBP radial scan from $\rho_{HIBP} = 1$ at LFS to $\rho_{HIBP} = -1$ at HFS: (a) and (b) power spectrograms of HIBP plasma density; (c) amplitudes of the perturbed plasma density; (d) and (e) power spectrograms of plasma potential; (f) amplitude of the perturbed plasma potential; (g) eigenfunction for the potential perturbation at $t = 1128$ ms, calculated by the FAR3D code.

electrostatic potential calculated by FAR3D. Positive and negative mode numbers show the combinations of sine and cosine components according to the FAR3D convention.[42] The simulations include the dynamic modes $n = 8$, $m = 3, 4, 5, 6$, and $n = -8$, $m = -3, -4, -5, -6$. The eigenfunction is localized at $(0.6 < \rho < 0.9)$, which is the outer part of the observed AELM radial extent within experimental uncertainties.

Among two modes, obtained with (1–3) for AELM, both reproducing the observed frequency evolution, the mode $m/n = 5/8$ at $\rho_{AELM} = 0.7$ better matches the observed radial location for the AELM. On top of that, it fits the core of the mode radial location, obtained by FAR3D.

Here, we should mention that the modeling of the long-lasting (several dozens of ms) AEs like AELM claims more precise knowledge of the spatial–temporal iota distribution. Modeling results are very sensitive to the fine details of the iota profile at any time slot. This also holds for density and temperature profiles, but to a less degree. As we do not have data of the real iota profile, deviations could exist between the iota profile in the simulations and in the real plasma at the middle–outer radial region. The consequence is slender AE gaps in STELLGAP (see Sec. IV) and mode eigenfunctions in FAR3D at the middle–outer plasma region, leading to the discrepancy between estimations (1–3) and FAR3D simulations on the one hand, and observations of AELM frequency and its extension on the other hand. Fitting of the f_{AELM} with Eqs. (1)–(3) allows us to compare the minimum of f_{AELM} equals to 62 ± 2 kHz with GAM frequency f_{GAM}. For f_{GAM} estimations, we use T_e profile (Fig. 2), $T_i = 0.1$ keV almost constant over the radius,[43] and the iota value $+\sim 1.6$ near its local minimum at $\rho = 0.2$–0.7. The frequency f_{GAM}, representing the minima for f_{AELM}, corresponds to $\rho_{GAM} = 0.4 \pm 0.1$, which is the maximum of the density perturbations, see Figs. 7(a)–7(c), and the inner edge of the plasma potential perturbation, see Figs. 7(d)–7(f). For the maximum of the potential perturbation, f_{GAM} $(\rho = 0.6) = 51 \pm 4$ kHz being $\sim$18% below the minima for f_{AELM}.

Model (1–3) suggests the local GAM with variable frequency dependent on local T_e and ρ. However, experiments in several tokamaks show that GAM may not strictly follow the local dispersion relation (3) and may be radially extended.[44–46] If in considered experiment, GAM is nonlocal radially extended mode, born at the core area $\rho_{GAM} = 0.4$, and widened over the whole area of AELM extent, it can fit Eq. (1) over this area.

Figure 8 presents another example of the mode evolution due to I_{pl} variation. In this shot #33029, the mode exists about 30 ms. The mode frequency varies from 30 to 225 kHz, or by a factor of 7, which is a record for AEs in TJ-II. The radial location of the mode, obtained with the HIBP radial scan, gives $\rho_{AELM} = 0.6$–0.9. The mode 5/8 at $\rho_{AE} = 0.75$, modeled with (1–3), fits both the location of the mode and the frequency sweep, including the local minima of the mode frequency in the linear phase of I_{pl}. The GAM frequency is estimated as f_{GAM} $(\rho = 0.7) = 30 \pm 5$ kHz. Note that in this shot only one NBI operated, producing lower temperatures with respect to the case of AELM.

The amplitude of the density and potential perturbations for the AELM (Fig. 9) shows large peaks at $t \approx 1125$, 1140, 1160, and 1175 ms. The AELM perturbation amplitude almost disappears at $t \approx 1133$, 1147, 1170, and 1190 ms. Remarkably, the time trace of the AELM amplitude presents a close correlation to that of the mode

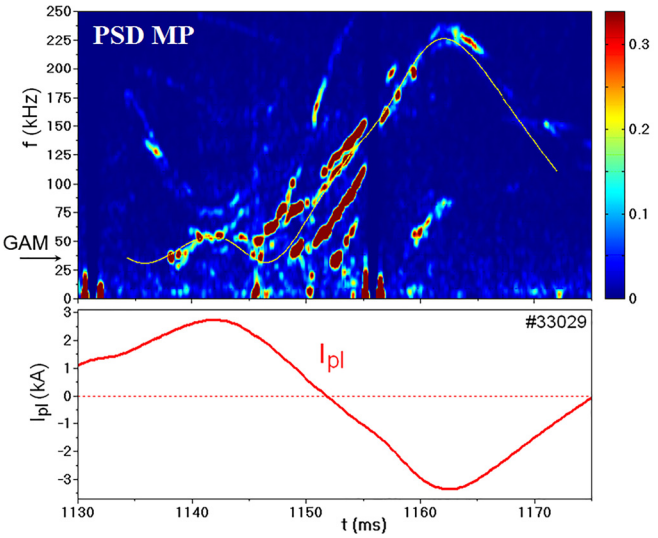

FIG. 8. The mode evolution in MP spectrogram and modeling of strong f_{AE} variation with I_{pl}, in a factor of 7; $f_{min} = f_{GAM} = 30$ kHz. The modeled mode 5/8@$\rho_{AE} = 0.75$ is shown in yellow.

frequency, f_{AELM}: the amplitudes of all oscillating quantities reach their minima, when f_{AELM} approaches f_{min}, and they tend to reach their maxima, when f_{AELM} approaches its maxima. The HIBP and MP signals in Fig. 9 also correlate with the evolution of the iota profile during the discharge: the local minima of the HIBP and MP signals and the AELM frequency take place simultaneously with the presence of the 8/5 rational surface, at $t \approx 1133$, 1147, 1170, and 1189 ms.

IV. NUMERICAL MODELING

We use the STELLGAP code[15] to calculate the Alfvén gaps for the evolving equilibria (iota profile) provided by the VMEC code.[18] The snapshots of the iota profile and the corresponding plasma current I_{pl} are shown in Fig. 2. We use them in the simulations of the AELM mode for the shot #33706.

Figure 10 presents the snapshots of the continuum gaps in the discharge #33706 for the toroidal mode numbers from $n = 3$ to 17. These STELLGAP calculations include the effect of helical couplings, as shown in Table I. Figure 10 shows that AELM represented as magenta line segment at AELM frequency and radial extent for plasma potential shown in Figs. 7(d)–7(f) is located near the local minima/maxima for the Alfvén continuum of the $n = 8$ toroidal family, marked by thick olive lines. Consequently, if the 5/8 helicity is the trigger of the AELM, this instability could be a global AE (GAE),[2] because the GAEs are extremal modes destabilized nearby the local minima/maxima of the Alfvén continuum.

To calculate the AELM frequency, we use an initial value version of the code FAR3D.[17] The code solves the reduced linear resistive MHD equations for the thermal plasma and the equations for the energetic ion density and parallel velocity. It uses appropriate closure relations to model the linear wave–particle resonance effects responsible for Landau damping/growth, as well as the compressibility of the thermal plasma to describe GAMs.

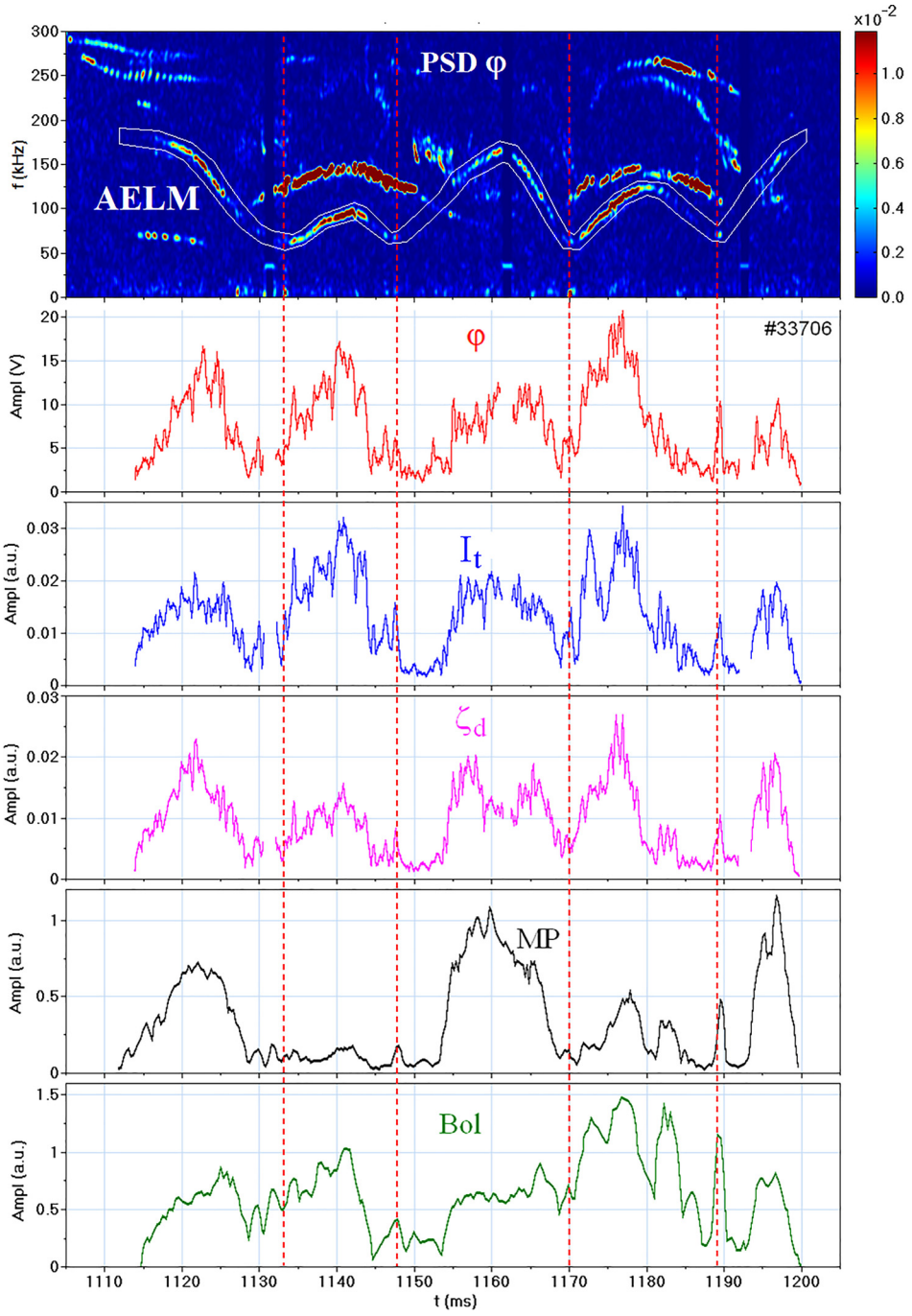

FIG. 9. Power spectrogram of plasma potential (upper box) and time evolution of the AELM amplitude of the perturbation of plasma parameters: potential, density, and magnetic potential by HIBP measured at a fixed position $\rho_{HIBP} = 0.35$, magnetic oscillations by MP, plasma emissivity by bolometer at $\rho_{Bol} = 0.1$. The oscillating quantities evolve coherently: the mode amplitude decreases, when f_{AELM} approaches f_{min}, as marked by vertical dashed lines. Thin white lines in the upper box designate the zone for AELM amplitude calculation.

No information on the energetic particle (EP) distribution function was available for the analysis. We, therefore, performed a parametric study for a range of the fast particle energies T_f, their normalized pressure β_f and density profiles n_f in order to match the AELM frequency sweeping observed in the experiment, following the procedure described in Ref. 39. First, we run FAR3D changing the EP energy in the range of $T_f = 5.8$–16 keV between $t = 1110$–1155 ms (fixed the β_f and n_f profile), selecting the T_f that triggers an AE with a frequency similar to the experimental observations. Next, we scan different β_f values between 0.001 and 0.03 (for the selected T_f and fixed n_f), selecting β_f that triggers an instability with a similar frequency range and the same evolution (up/down sweeping) regarding the experimental observations. Finally, fixed β_f and T_f, we perform a fine tuning of the n_f profile by changing the intensity and radial location of the n_f gradient.

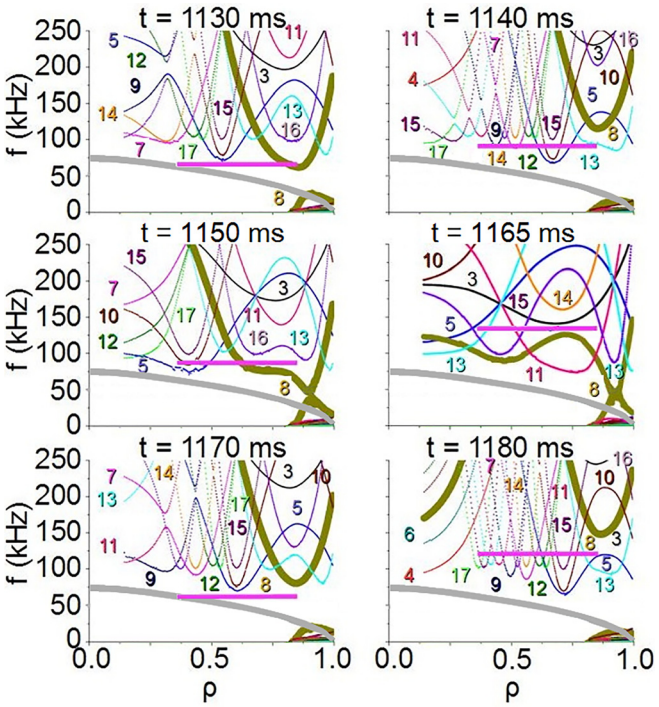

FIG. 10. Alfvén gaps structure toward the discharge # 33706 of the $n = 3$–17 toroidal mode families including the effect of the helical couplings. The colored lines indicate the toroidal mode numbers. The fat gray lines indicate GAM frequency, estimated with Eq. (3), and the magenta solid lines indicate the observed AELM frequency and radial extent for plasma potential perturbations. AELM is consistent with the gap of the Alfvén continuum caused by $n = 8$ toroidal family indicated by the thick olive line.

The best fit was obtained for $T_f = 5.8$ keV (no radial dependence), $\beta_f = 0.0025$, and the n_f profile shown in Fig. 11, fixed for all times in our simulations. The EP density gradient is located at $(0.6 < \rho < 0.9)$; that is, the outer edge of the AELM destabilization region measured in the experiment. The energy $T_f = 5.8$ keV is 1/3 of the effective energy of the fast particles $T_{f,e}$ calculated as $T_{f,e} = 0.573 \cdot E_{NBI}$.[17]

The evolution of the frequency of the dominant member of $n = 8$ toroidal family, the mode $m/n = 5/8$, calculated by the FAR3D code is shown in Fig. 6(b) and the mode eigenfunction in Fig. 7(g).

TABLE I. Toroidal and poloidal mode numbers in the STELLGAP simulations.

n	m	n	m
3	1–8	10	2–16
4	1–10	11	2–16
5	1–10	12	3–18
6	1–12	13	3–18
7	1–12	14	3–20
8	2–14	15	3–20
9	2–14	16	4–22
…	…	17	4–22

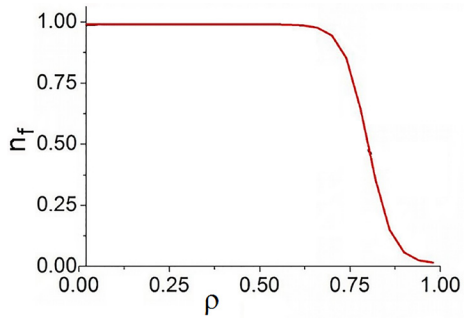

FIG. 11. Normalized fast particle density profile.

The code reasonably reproduces the tendency of frequency variation, but the calculated frequency is sometimes higher than the experimental one, shown in Fig. 6(a). It could be that the disagreement is caused by errors in the reconstruction of the iota profile and the uncertainty in the thermal plasma and EP radial profiles. The calculated eigenfunctions for plasma potential perturbation $(0.6 < \rho < 0.9)$ are placed at the outer edge of the localization of potential and density perturbations, caused by AELM, as shown in Fig. 7. We thus observe that the results of both STELLGAP and FAR3D show the $m/n = 5/8$ mode as the closest to AELM in frequency value, temporal evolution, and radial location.

For the iota profiles included in the model, the AE gaps calculated by STELLGAP in the frequency range compared with the experiments are quite narrow and located in the middle–outer plasma region, leading also to a narrow eigenfunction located at the middle–outer plasma in FAR3D simulations regarding the observations. If more accurate iota profile would allow the AE gap to be wider as well as the AELM eigenfunction, this would lead to a better agreement with the perturbed potential and density data.

V. SUMMARY

We have conducted an extended set of experiments with varying ι profiles in NBI plasmas of the TJ-II flexible heliac. Adjustable plasma current I_{pl} enables the variations in ι. A few kA variation of the plasma current changes the mode frequency dramatically: f_{AE} decreases (increases) up to a factor of 7. We observe that (i) f_{AE} has a lower limit approaching the local GAM frequency, and (ii) the mode amplitude evolves in step with I_{pl}, increasing with f_{AE} up to its maximum and decreasing with f_{AE} up to its minimum. A simple analytical estimation[10] for f_{AE} with mode numbers m, n describes the observations, particularly, when I_{pl} causes iota to have rational value m/n at the mode location. In these cases, the mode parallel wave-vector vanishes, and frequency has a minimum value close to f_{GAM}. Modeling with the STELLGAP and FAR3D codes reproduces the AE frequency sweep caused by the plasma current I_{pl} variation and the mode numbers of the analytical model. The codes also show that the minimal frequency of the simulated mode is close to the observed value, while the simulated eigenfunction is located at the outer edge of the observed mode.

ACKNOWLEDGMENTS

The work is a result of the long-term cooperation between participating institutes. The research and data analysis done by the

Kurchatov team in Secs. II and III were funded by the Russian Science Foundation, Project No. 19-12-00312. J.V. was supported by the Comunidad de Madrid, Grant No. 2019-T1/AMB-13648. The CIEMAT team was supported by the Comunidad de Madrid, Grant No. Y2018/NMT (PROMETEO-CM). B.N.B. was supported by the U.S. Department of Energy Contract No. DEFG02–04ER54742.

DATA AVAILABILITY

The data that support the findings of this study are available from the corresponding author upon request.

REFERENCES

[1]N. N. Gorelenkov, S. D. Pinches, and K. Toi, "Energetic particle physics in fusion research in preparation for burning plasma experiments," Nucl. Fusion **54**, 125001 (2014).
[2]W. W. Heidbrink, "Basic physics of Alfvén instabilities driven by energetic particles," Phys. Plasmas **15**, 055501 (2008).
[3]B. N. Breizman and S. E. Sharapov, "Major minority: Energetic particles in fusion plasmas," Plasma Phys. Controlled Fusion **53**, 054001 (2011).
[4]K. Nagaoka, T. Ido, E. Ascasíbar, T. Estrada, S. Yamamoto, A. V. Melnikov, A. Cappa, C. Hidalgo, M. A. Pedrosa, B. P. van Milligen *et al.*, "Mitigation of NBI driven Alfvén eigenmodes by electron cyclotron heating in the TJ-II stellarator," Nucl. Fusion **53**, 072004 (2013).
[5]A. V. Melnikov, L. G. Eliseev, R. Jiménez-Gómez, E. Ascasibar, C. Hidalgo, A. A. Chmyga, T. Ido, S. M. Khrebtov, A. Könies, A. D. Komarov *et al.*, "Study of Alfvén eigenmodes in the TJ-II stellarator," Plasma Fusion Res. **5**, S2019 (2010).
[6]M. Garcia-Munoz, S. E. Sharapov, M. A. van Zeeland, E. Ascasibar, A. Cappa, L. Chen, J. Ferreira, J. Galdon-Quiroga, B. Geiger, J. Gonzalez-Martin *et al.*, "Active control of Alfvén eigenmodes in magnetically confined toroidal plasmas," Plasma Phys. Controlled Fusion **61**, 054007 (2019).
[7]S. Yamamoto, K. Nagasaki, K. Nagaoka, J. Varela, Á. Cappa, E. Ascasíbar, F. Castejón, J. M. Fontdecaba, J. M. García-Regaña, Á. González-Jerez *et al.*, "Effect of ECH/ECCD on energetic-particle-driven MHD modes in helical plasmas," Nucl. Fusion **60**, 066018 (2020).
[8]A. V. Melnikov, L. G. Eliseev, E. Ascasibar, A. A. Chmyga, C. Hidalgo, T. Ido, R. Jiménez-Gómez, I. A. Krasilnikov, A. D. Komarov, A. S. Kozachek *et al.*, "Alfvén eigenmodes properties and dynamics in the TJ-II stellarator," Nucl. Fusion **52**, 123004 (2012).
[9]M. Ochando, D. López-Bruna, F. Medina, A. Cappa, E. Ascasíbar, A. López-Fraguas, S. Yamamoto, and TJ-II Team, "Plasma current dependence of coherent modes frequency in low-density NBI heated discharges in the TJ-II stellarator," in Proceedings of 39th EPS Conference and 16th Congress on Plasma Physics, ECA, Stockholm, Sweden, 2–6 July (2012), Vol. 36F, p. P4.063.
[10]B. N. Breizman, M. S. Pekker, and S. E. Sharapov, "Plasma pressure effect on Alfvén cascade eigenmodes," Phys. Plasmas **12**, 112506 (2005).
[11]M. A. Van Zeeland, W. W. Heidbrink, S. E. Sharapov, D. Spong, A. Cappa, X. Chen, C. Collins, M. García-Muñoz, N. N. Gorelenkov, G. J. Kramer *et al.*, "Electron cyclotron heating can drastically alter reversed shear Alfvén eigenmode activity in DIII-D through finite pressure effects," Nucl. Fusion **56**, 112007 (2016).
[12]E. M. Bass and R. E. Waltz, "Gyrokinetic simulation of global and local Alfvén eigenmodes driven by energetic particles in a DIII-D discharge," Phys. Plasmas **20**, 012508 (2013).
[13]K. Toi, F. Watanabe, T. Tokuzawa, K. Ida, S. Morita, T. Ido, A. Shimizu, M. Isobe, K. Ogawa, D. A. Spong *et al.*, "Observation of reversed-shear Alfvén eigenmodes excited by energetic ions in a helical plasma," Phys. Rev. Lett. **105**, 145003 (2010).
[14]A. V. Melnikov, L. G. Eliseev, R. Jiménez-Gómez, E. Ascasibar, C. Hidalgo, A. A. Chmyga, A. D. Komarov, A. S. Kozachok, I. A. Krasilnikov, S. M. Khrebtov *et al.*, "Internal measurements of Alfvén eigenmodes with heavy ion beam probing in toroidal plasmas," Nucl. Fusion **50**, 084023 (2010).
[15]D. A. Spong, R. Sanchez, and A. Weller, "Shear Alfvén continua in stellarators," Phys. Plasmas **10**, 3217 (2003).
[16]L. Garcia, "Global stability of stellarator configurations," in Proceedings of ICPP and 25th EPS Conference Controlled Fusion and Plasma Physics, ECA, Praha, Czech Republic, 29 June–3 July (1998), Vol. 22C, p. 1757.
[17]J. Varela, K. Y. Watanabe, K. Shinohara, M. Honda, Y. Suzuki, J. Shiraishi, D. A. Spong, and L. Garcia, "MHD stability of JT-SA operation scenarios driven by passing energetic-particles for a hot Maxwellian model," Nucl. Fusion **60**, 096009 (2020).
[18]S. P. Hirshman and J. C. Whitson, "Steepest-descent moment method for three-dimensional magnetohydrodynamic equilibria," Phys. Fluids **26**, 3553 (1983).
[19]C. Hidalgo, M. A. Pedrosa, N. Dreval, K. J. McCarthy, L. Eliseev, M. A. Ochando, T. Estrada, I. Pastor, E. Ascasíbar, E. Calderón *et al.*, "Improved confinement regimes induced by limiter biasing in the TJ-II stellarator," Plasma Phys. Controlled Fusion **46**, 287 (2004).
[20]A. V. Melnikov, M. Ochando, E. Ascasibar, F. Castejon, A. Cappa, L. G. Eliseev, C. Hidalgo, L. I. Krupnik, A. Lopez-Fraguas, M. Liniers *et al.*, "Effect of magnetic configuration on frequency of NBI-driven Alfvén modes in TJ-II," Nucl. Fusion **54**, 123002 (2014).
[21]D. López-Bruna, F. Castejón, T. Estrada, J. A. Romero, J. A. Jiménez, E. Ascasíbar, and TJ-II Team, "Effects of Ohmic current in the TJ-II stellarator," Nucl. Fusion **44**, 645 (2004).
[22]A. V. Melnikov, L. G. Eliseev, E. Ascasibar, A. Cappa, F. Castejon, C. Hidalgo, T. Ido, J. A. Jimenez, A. S. Kozachek, L. I. Krupnik *et al.*, "Transition from chirping to steady NBI-driven Alfvén modes caused by magnetic configuration variations in the TJ-II stellarator," Nucl. Fusion **56**, 076001 (2016).
[23]F. Castejón, M. de Aguilera, E. Ascasíbar, T. Estrada, C. Hidalgo, A. López-Fraguas, M. A. Ochando, S. Yamamoto, A. V. Melnikov, L. G. Eliseev *et al.*, "Influence of magnetic well on electromagnetic turbulence in the TJ-II stellarator," Plasma Phys. Controlled Fusion **58**, 094001 (2016).
[24]A. V. Melnikov, L. G. Eliseev, F. Castejón, C. Hidalgo, P. O. Khabanov, A. S. Kozachek, L. I. Krupnik, M. Liniers, S. E. Lysenko, J. L. de Pablos *et al.*, "Study of NBI-driven chirping mode properties and radial location by the heavy ion beam probe in the TJ-II stellarator," Nucl. Fusion **56**, 112019 (2016).
[25]J. Sánchez, M. Acedo, A. Alonso, J. Alonso, P. Alvarez, E. Ascasibar, A. Baciero, R. Balbin, L. Barrera, E. Blanco *et al.*, "Confinement transitions in TJ-II under Li-coated wall conditions," Nucl. Fusion **49**, 104018 (2009).
[26]M. Liniers, J. Damba, J. Guasp, J. A. Sebastián, F. Martín, B. Rojo, R. Carrasco, E. Sánchez, F. Miguel, G. Wolfers *et al.*, "Beam transmission dependence on beam parameters for TJ-II neutral beam injectors," Fusion Eng. Des. **123**, 259 (2017).
[27]F. Castejón, D. Alegre, A. Alonso, J. Alonso, E. Ascasíbar, A. Baciero, A. de Bustos, D. Baiao, J. M. Barcala, E. Blanco *et al.*, "3D effects on transport and plasma control in the TJ-II stellarator," Nucl. Fusion **57**, 102022 (2017).
[28]R. Jiménez-Gómez, E. Ascasíbar, T. Estrada, I. García-Cortés, B. van Milligen, A. López-Fraguas, I. Pastor, and D. López-Bruna, "Analysis of magnetohydrodynamic instabilities in TJ-II plasmas," Fusion Sci. Technol. **51**, 20 (2007).
[29]M. A. Ochando, F. Medina, B. Zurro, A. Baciero, K. J. McCarthy, M. A. Pedrosa, C. Hidalgo, E. Sánchez, J. Vega, A. B. Portas *et al.*, "Up-down and in-out asymmetry monitoring based on broadband radiation detectors," Fusion Sci. Technol. **50**, 313 (2006).
[30]Y. N. Dnestrovskij, A. V. Melnikov, L. I. Krupnik, and I. S. Nedzelskij, "Development of heavy ion beam probe diagnostics," IEEE Trans. Plasma Sci. **22**, 310 (1994).
[31]A. J. H. Donné, A. V. Melnikov, and G. van Oost, "Diagnostics for radial electric field measurements in hot magnetized plasmas," Czech. J. Phys. **52**, 1077 (2002).
[32]I. S. Bondarenko, A. A. Chmuga, N. B. Dreval, S. M. Khrebtov, A. D. Komarov, A. S. Kozachok, L. I. Krupnik, P. Coelho, M. Cunha, B. Gonçalves *et al.*, "Installation of an advanced heavy ion beam diagnostic on the TJ-II stellarator," Rev. Sci. Instrum. **72**, 583 (2001).
[33]A. V. Melnikov, L. I. Krupnik, E. Ascasibar, A. Cappa, A. A. Chmyga, G. N. Deshko, M. A. Drabinskij, L. G. Eliseev, C. Hidalgo, P. O. Khabanov *et al.*, "ECRH effect on the electric potential and turbulence in the TJ-II stellarator and T-10 tokamak plasmas," Plasma Phys. Controlled Fusion **60**, 084008 (2018).
[34]A. V. Melnikov, "Applied and fundamental aspects of fusion science," Nat. Phys. **12**, 386 (2016).

[35]A. V. Melnikov, L. I. Krupnik, L. G. Eliseev, J. M. Barcala, A. Bravo, A. A. Chmyga, G. N. Deshko, M. A. Drabinskij, C. Hidalgo, P. O. Khabanov *et al.*, "Heavy ion beam probing—diagnostics to study potential and turbulence in toroidal plasmas," Nucl. Fusion **57**, 072004 (2017).
[36]P. O. Khabanov, L. G. Eliseev, A. V. Melnikov, M. A. Drabinskij, C. Hidalgo, N. K. Kharchev, A. A. Chmyga, A. S. Kozachek, I. Pastor, J. L. de Pablos *et al.*, "Density profile reconstruction using HIBP in ECRH plasmas in the TJ-II stellarator," J. Instrum. **14**, C09033 (2019).
[37]A. V. Melnikov, *Electric Potential in Toroidal Plasmas* (Springer Nature Switzerland AG, 2019), pp. 1–240.
[38]V. A. Mazur and A. B. Mikhajlovskij, "Stabilization of the Alfvén wave instability in a two-component tokamak," Nucl. Fusion **17**, 193 (1977).
[39]J. L. Velasco and F. Castejon, "Study of the neoclassical radial electric field of the TJ-II flexible heliac," Plasma Phys. Controlled Fusion **54**, 015005 (2012).
[40]H. Sugama and T.-H. Watanabe, "Collisionless damping of zonal flows in helical systems," Phys. Plasmas **13**, 012501 (2006).
[41]T. Watari, Y. Hamada, T. Notake, N. Takeuchi, and K. Itoh, "Geodesic acoustic mode oscillation in the low frequency range," Phys. Plasmas **12**, 062304 (2005).
[42]J. Varela, D. A. Spong, L. Garcia, Y. Todo, J. Huang, and M. Murakami, "Study of Alfven eigenmodes stability in plasma with multiple NBI driven energetic particle species," Phys. Plasmas **26**, 062502 (2019).
[43]E. Ascasibar, D. Alba, D. Alegre, A. Alonso, J. Alonso, F. de Aragón, A. Baciero, J. M. Barcala, E. Blanco, J. Botija *et al.*, "Overview of recent TJ-II stellarator results," Nucl. Fusion **59**, 112019 (2019).
[44]T. Ido, Y. Miura, K. Kamiya, Y. Hamada, K. Hoshino, A. Fujisawa, K. Itoh, S.-I. Itoh, A. Nishizawa, H. Ogawa *et al.*, "Geodesic–acoustic-mode in JFT-2M tokamak plasmas," Plasma Phys. Controlled Fusion **48**, S41 (2006).
[45]C. A. de Mejere, S. Coda, Z. Huang, L. Vermare, T. Vernay, V. Vuille, S. Brunner, J. Dominski, P. Hennequin, A. Krämer-Flecken *et al.*, "Complete multi-field characterization of the geodesic acoustic mode in the TCV tokamak," Plasma Phys. Controlled Fusion **56**, 072001 (2014).
[46]A. V. Melnikov, L. G. Eliseev, S. V. Perfilov, S. E. Lysenko, R. V. Shurygin, V. N. Zenin, S. A. Grashin, L. I. Krupnik, A. S. Kozachek, R. Y. Solomatin *et al.*, "The features of the global GAM in OH and ECRH plasmas in the T-10 tokamak," Nucl. Fusion **55**, 063001 (2015).